Available online at www.sciencedirect.com

ScienceDirect

Ceramics International 40 (2014) 5079–5084

CERAMICS INTERNATIONAL

www.elsevier.com/locate/ceramint

Short communication

Fabrication and properties of porous Si_3N_4–SiO_2 ceramics with dense surface and gradient pore distribution

Xiangming Li, Pute Wu*, Delan Zhu

Institute of Water Saving Agriculture in Arid Areas of China, Northwest A&F University, Yangling, Shaanxi 712100, PR China

Received 1 September 2013; received in revised form 15 September 2013; accepted 15 September 2013
Available online 23 September 2013

Abstract

For fabricating porous Si_3N_4–SiO_2 ceramics with good moisture resistance and mechanical and dielectric properties, a technique combining oxidation–bonding, sol–gel directional infiltration and sintering is explored. The sol–gel infiltration time has great effect on the microstructure and properties of the porous Si_3N_4–SiO_2 ceramics. As the infiltration time increases, the porous Si_3N_4–SiO_2 ceramics improve obviously in mechanical properties and decline little in dielectric properties. With the increase of infiltration time from 0.5 to 2.0 h, the porous Si_3N_4–SiO_2 ceramics increase obviously in flexural strength from 46 to 121 MPa and in Vickers hardness from 2.4 to 5.3 GPa, increase slightly in dielectric constant from 3.32 to 3.76 and in dielectric loss from 3.36×10^{-3} to 3.65×10^{-3}. Due to their dense surface, the porous Si_3N_4–SiO_2 ceramics possess good resistances to moisture and mechanical shock.

Keywords: C. Dielectric properties; C. Mechanical properties; D. Si_3N_4; Porous; Moisture resistance

1. Introduction

The radomes and antenna windows used in carrier rockets, airships, missiles and return satellites are made of excellent electromagnetic wave transparent materials possessing good mechanical and dielectric properties [1]. SiO_2 and Si_3N_4 are two potential materials used for fabricating the electromagnetic wave transparent materials [2–4], but the poor mechanical properties of SiO_2 [5,6] and the high dielectric constant of Si_3N_4 limit their application as radomes or antenna windows [3,4]. Synthesizing Si_3N_4–SiO_2 ceramics may retain good mechanical properties of Si_3N_4 and good dielectric properties of SiO_2 meanwhile, and the Si_3N_4–SiO_2 ceramics improve further in dielectric properties by increasing porosity [1,7]. So far, various techniques have been developed to fabricate porous Si_3N_4–SiO_2 ceramics, and the mechanical and dielectric properties of porous Si_3N_4–SiO_2 ceramics have been studied extensively. However, the porous Si_3N_4–SiO_2 ceramics will absorb moisture when used in a moist environment especially in rain [8,9]. Due to the high dielectric constant of water (78.36 at 25 °C), radomes or antenna windows fabricated from porous Si_3N_4–SiO_2 ceramics will deteriorate dramatically in dielectric properties after absorbing moisture. Until now, there is a lack of research about improving the moisture resistance of porous Si_3N_4–SiO_2 ceramics.

Revealed from our previous work [8,9], dense surface with a porous internal structure brings meanwhile good moisture resistance and dielectric properties to porous Si_3N_4 ceramics. In the present work, focusing on improving the moisture resistance of porous Si_3N_4–SiO_2 ceramics, a technique combining oxidation–bonding, sol–gel directional infiltration and sintering is explored to fabricate porous Si_3N_4–SiO_2 ceramics with a dense surface and gradient pore distribution. The effects of the sol–gel infiltration time on the microstructure, mechanical and dielectric properties of the porous Si_3N_4–SiO_2 ceramics are discussed in detail.

2. Experimental procedure

2.1. Fabrication techniques

Si_3N_4 powder (α ratio > 90 wt%, purity > 99.9%, mean particle size of 0.7 μm, Corefra Materials Co., Ltd. Hebei,

*Corresponding author. Tel.: +86 29 87092860; fax: +86 29 87012210.
E-mail addresses: li_xiangming@yahoo.com, gjzwpt@vip.sina.com (P. Wu).

0272-8842/$ - see front matter © 2013 Elsevier Ltd and Techna Group S.r.l. All rights reserved.
http://dx.doi.org/10.1016/j.ceramint.2013.09.068

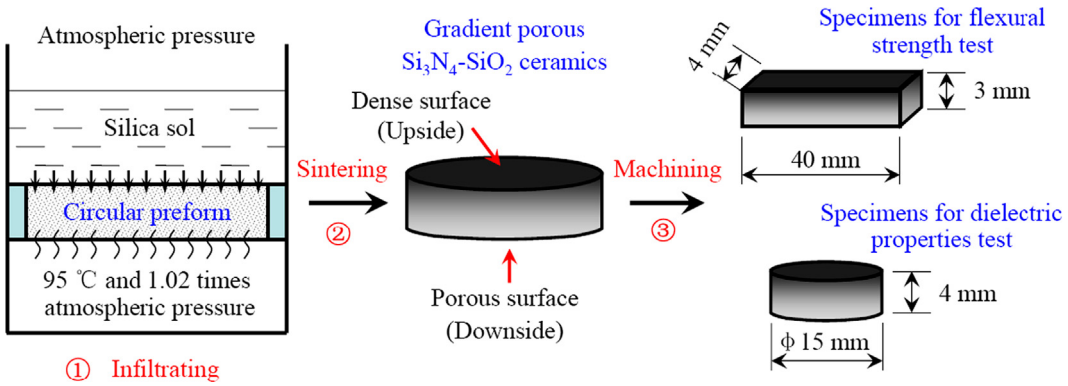

Fig. 1. Schematic of the fabrication process of porous Si_3N_4–SiO_2 ceramics with dense surface and gradient pore distribution.

China) was mixed with 10 wt% dextrin, and then ball-milled for 10 h. The powder blend was cold-pressed into green bodies with a dimension of 30 mm × 50 mm diameter, and then sintered into porous Si_3N_4–SiO_2 ceramic preforms by oxidizing in air at 1200–1300 °C for 2 h. The preforms were machined into circular specimens with a dimension of 4 mm × 45 mm diameter, and then assembled in a device shown in Fig. 1 to infiltrate silica sol (SiO_2 = 30 ± 1%, mean grain size of 10–20 nm, viscosity ≤ 7 mpa s, Na_2O ≤ 0.06%, pH = 7.5–8.5, Yinke Materials Co., Ltd. Zibo, China) directionally for 0.5, 1.0 and 2.0 h. According to the results of preliminary experiments, the optimal temperature and pressure in the chamber at the bottom of the device is determined at 95 °C and 1.02 times atmospheric pressure. After the sol–gel infiltration process, the preforms were sintered in nitrogen at 1250 °C for 2 h. Finally, according to the schematic shown in Fig. 1, the porous Si_3N_4–SiO_2 ceramics were machined into specimens with dimensions of 3 mm × 4 mm × 40 mm for flexural strength test and 4 mm × 15 mm diameter for dielectric properties test.

2.2. Characterization and tests

Phase analysis was conducted by X-ray diffraction (XRD). Microstructure was observed by scanning electron microscopy (SEM). Porosity was measured by the Archimedes method. Flexural strength (σ) was measured via the three-point bending test with a support distance of 30 mm. Vickers hardness (Hv) was measured using a digital hardness tester with a pyramidal Vickers indenter. Dielectric constant and loss was measured at 14 GHz by a resonant cavity method using the TE_{01d} mode examined by a vector network analyzer (Hewlett–Packard Hp8720ES) with a 1 Hz resolution.

For the convenience of the following discussion, the porous Si_3N_4–SiO_2 ceramics fabricated via different times of sol–gel directional infiltration are named as SN-n (n stands for the infiltration time).

3. Results and discussion

The mechanical properties of the porous Si_3N_4–SiO_2 ceramics have much to do with the properties of the preforms, so

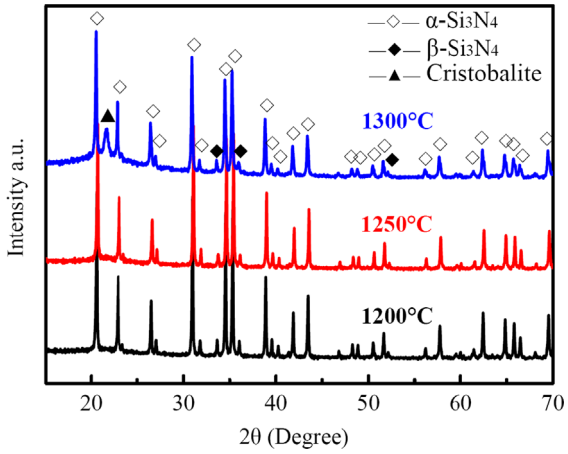

Fig. 2. XRD patterns of the porous Si_3N_4–SiO_2 ceramic preforms oxidized at 1200–1300 °C for 2 h.

the optimal temperature for preform fabrication should be first determined. During the oxidation process, the dextrin in the green bodies is oxidized and removed, and the Si_3N_4 particles are bonded by SiO_2 deriving from the oxidation of Si_3N_4. The oxidation product of Si_3N_4 is an amorphous SiO_2 at lower temperature, and turns into cristobalite as the temperature rises [10]. Fig. 2 shows the XRD patterns of the preforms oxidized at different temperatures. When the temperature is below 1250 °C, no cristobalite peak is found and the oxidation product is only amorphous SiO_2. As the temperature reaches 1300 °C, the cristobalite peaks appeared.

Table 1 shows the properties of the preforms oxidized at different temperatures. As the temperature rises from 1200 to 1300 °C, the preforms increase in the oxidation degree of Si_3N_4 from 35.6 to 47.5% and in volume shrinkage from 0.6 to 1.1% but decrease in the total porosity from 50.3 to 40.7% and in the open porosity from 50.1 to 36.9%. After oxidizing at 1300 °C, due to the highest oxidation degree of Si_3N_4 and lowest total porosity of the preforms, the Si_3N_4 particles in the preforms are bonded strongly by SiO_2, so the preforms oxidizing at 1300 °C theoretically have the highest flexural strength. However, due to the large CTE mismatch between Si_3N_4 and cristobalite [4,11], the overmuch cristobalite induces the formation of micro-cracks during the oxidation process and

Table 1
Oxidation degree of Si_3N_4, porosity, volume shrinkage and flexural strength of the porous Si_3N_4–SiO_2 ceramic preforms oxidized at 1200–1300 °C for 2 h.

Temperature (°C)	Oxidation degree of Si_3N_4 (%)	Porosity (%)		Volume shrinkage (%)	σ (MPa)
		Total	Open		
1200	35.6	50.3	50.1	0.6	13
1250	38.7	43.1	42.5	0.7	22
1300	47.5	40.7	36.9	1.1	24

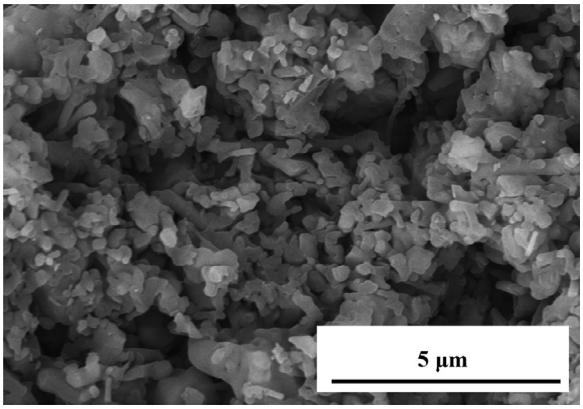

Fig. 3. SEM micrograph of the porous Si_3N_4–SiO_2 ceramic preforms oxidized at 1250 °C for 2 h.

then decrease the flexural strength of the preforms. As indicated in Table 1, the preforms oxidizing at 1250 and 1300 °C have almost the same flexural strength. According to the above results, for remaining high open porosity of the preforms and avoiding the crystallization of SiO_2 in the porous Si_3N_4–SiO_2 ceramics, 1250 °C is selected for the oxidation–bonding process.

Fig. 3 shows the SEM micrograph of the preforms oxidized at 1250 °C. As can be seen, the Si_3N_4 particles in the preforms are bonded weakly with each other, and the bonding necks between the Si_3N_4 particles are fine. There is no crack detected and the pores among the Si_3N_4 particles connect well with each other. The well-connected pores are the releasing channel of nitrogen during the oxidation process, and thereafter act as the transferring channel of silica sol during the sol–gel infiltration process [7].

As shown in Fig. 1, at the beginning of the sol–gel infiltration process, the silica sol enters into the open pores at the upside surface of the preforms, and then transfers downwards along the well-connected pores. Because of the little higher pressure at the downside surface of the preforms, the transferring speed of silica sol in the preforms is low. Due to the relative high temperature of the preforms, the silica sol transferring along the well-connected pores turns into silica gel little by little, and the silica gel deposits on the surface of the well-connected pores. As time increases, the pore size of the preforms decreases gradually due to the accumulation of silica gel, and the transferring speed of silica sol along the pore canals gets lower and lower. In that case, silica gel deposits mostly in the pores at the upside of the preforms with very little in the pores at the downside of the preforms. As the pore canals are blocked by silica gel, the silica sol could not transfer downwards anymore but deposit in the pores at the upside surface of the preforms. After the sol–gel infiltration process, the silica gel fills mostly in the pores at the upside surface of the preforms but very little in the pores at the downside of the preforms. By sintering the preforms in nitrogen at 1250 °C for 2 h, porous Si_3N_4–SiO_2 ceramics with dense surface and gradient pore distribution are obtained.

The oxidation of Si_3N_4 is a volume expansion process, and the Si_3N_4 particles in the green bodies are fixed quickly by oxidation-derived SiO_2 at the beginning of the oxidation process. Once the Si_3N_4 particles have been fixed by SiO_2, the dimension of green bodies will remain almost unchanged during the oxidation process [7], so the volume shrinkage of the preforms oxidized at 1250 °C is only 0.7%, as listed in Table 1. The sol infiltration technique of fabricating ceramics has many advantages, but the method suffers from the problem of shrinkage during drying and sintering process due to the removal of volatiles, leading to matrix cracking and residual fine pores in ceramics [12]. In the present work, the sol–gel infiltration is conducted at 95 °C, so silica sol turns into silica gel accompanied by the removal of volatiles during the sol–gel infiltration process. When sintering at 1250 °C, the silica gel in the pores near the upside surface of the preforms turns into amorphous SiO_2 quickly, and then fuses with the original oxidation-derived SiO_2 at the surface of Si_3N_4 particles into whole one, blocking the original well-connected open pores into closed ones without the generation of residual fine pores. Moreover, due to the restriction of the spatial porous structure in the preforms, the fusion of the sol–gel-derived SiO_2 with original oxidation-derived SiO_2 results hardly in the shrinkage of porous Si_3N_4 ceramics.

Fig. 4(a–c) shows the micrographs of the fracture surface near the upside surface of SN-*n*. By comparing the three micrographs, with the increase of infiltration time from 0.5 to 2.0 h, the amount of silica gel depositing in the pores increases, and the well-connected pores among Si_3N_4 particles are blocked into separate ones with the pore size decreasing. As shown in Fig. 4(c), the microstructure near the upside surface of SN-2.0 is dense, Si_3N_4 particles are well-bonded by SiO_2 and difficult to be identified, few pores can be found, the pores are very small and distribute separately with each other. Fig. 4(d) shows the micrograph of fracture surface near the downside surface of SN-2.0. As can be seen, the

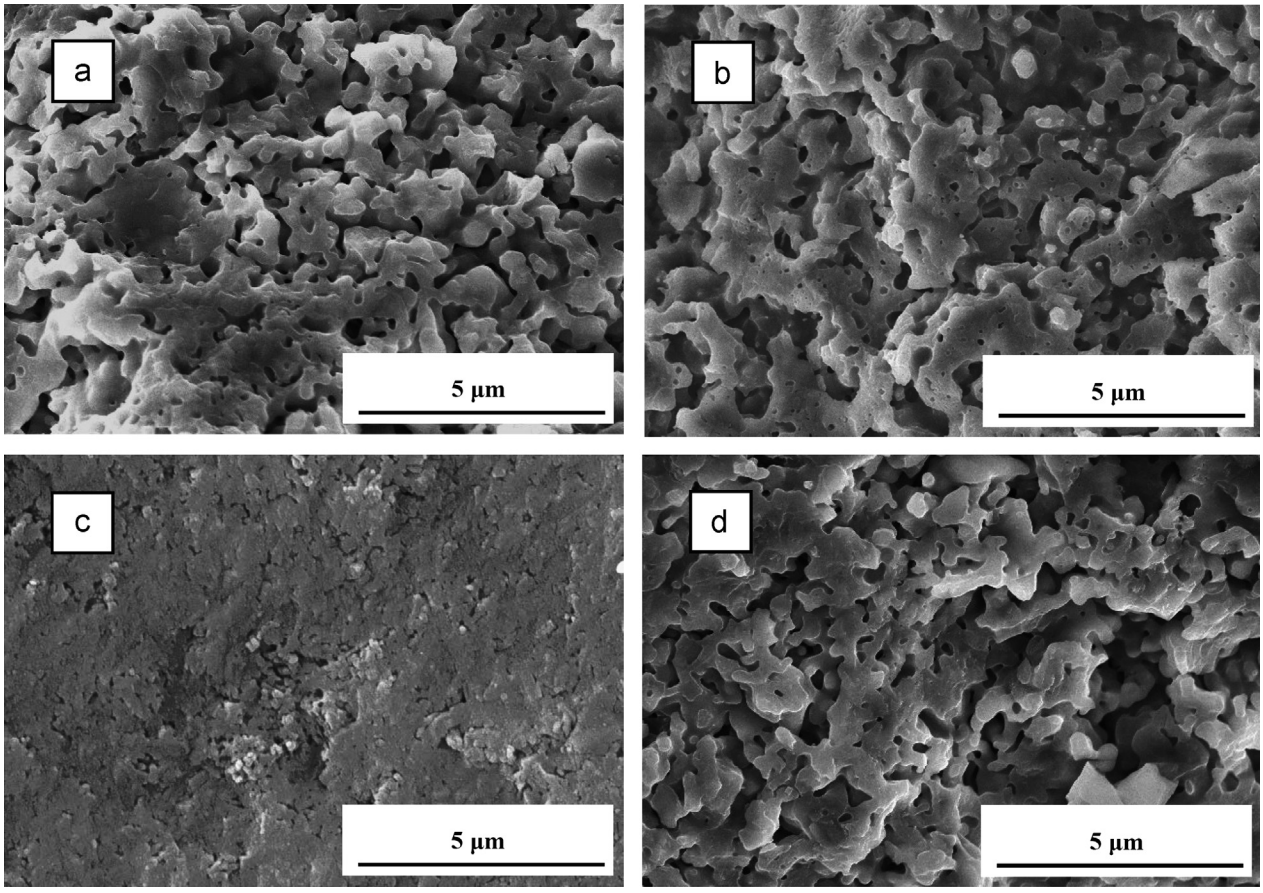

Fig. 4. SEM micrographs of the fracture surface near the upside surface of (a) SN-0.5, (b) SN-1.0 and (c) SN-2.0 and that near the downside surface of (d) SN-2.0.

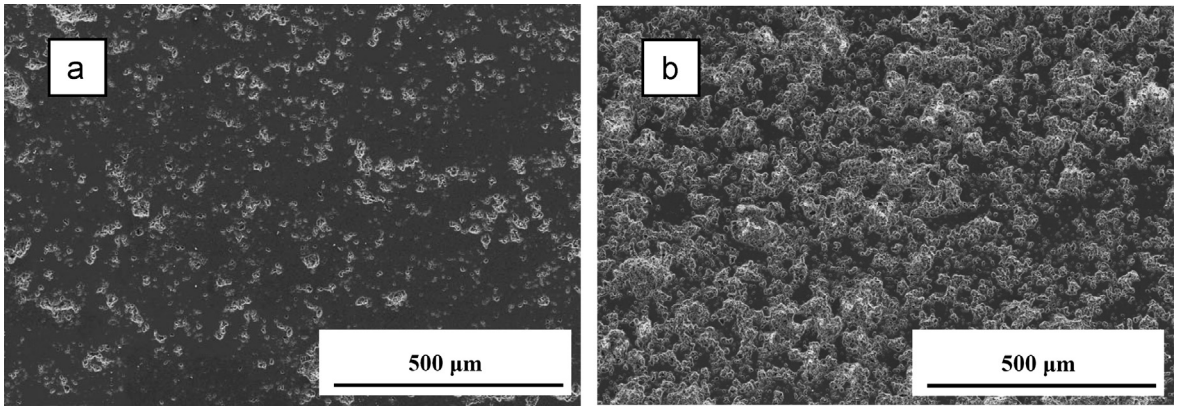

Fig. 5. SEM micrographs of the polished surface near the (a) upside and (b) downside surfaces of SN-2.0.

microstructure near the downside surface is porous and distinct from that near the upside surface, so it can be inferred with a reason that there is a gradient pore distribution in SN-2.0.

Fig. 5 also compares the micrographs of the polished surface near the upside surface and downside surface of SN-2.0, a great many well-connected pores can be seen clearly near the downside surface (Fig. 5(b)), so water can enter into SN-2.0 from the downside surface, while the pores near the upside surface are much fewer and distribute separately with each other (Fig. 5(a)), which means there is no connected pore canal for the moisture entering into the SN-2.0 from the upside surface.

Figs. 6 and 7 show the mechanical and dielectric properties of SN-*n*. As shown in Fig. 6(a), as the infiltration time increases from 0.5 to 2.0 h, the flexural strength of SN-*n* increases from 46 to 121 MPa when the dense surface of SN-*n* is downward during the test and increases from 37 to 62 MPa when the dense surface of SN-*n* is upward during test. During the infiltration process, as the well-connected pore canals have been blocked by silica gel,

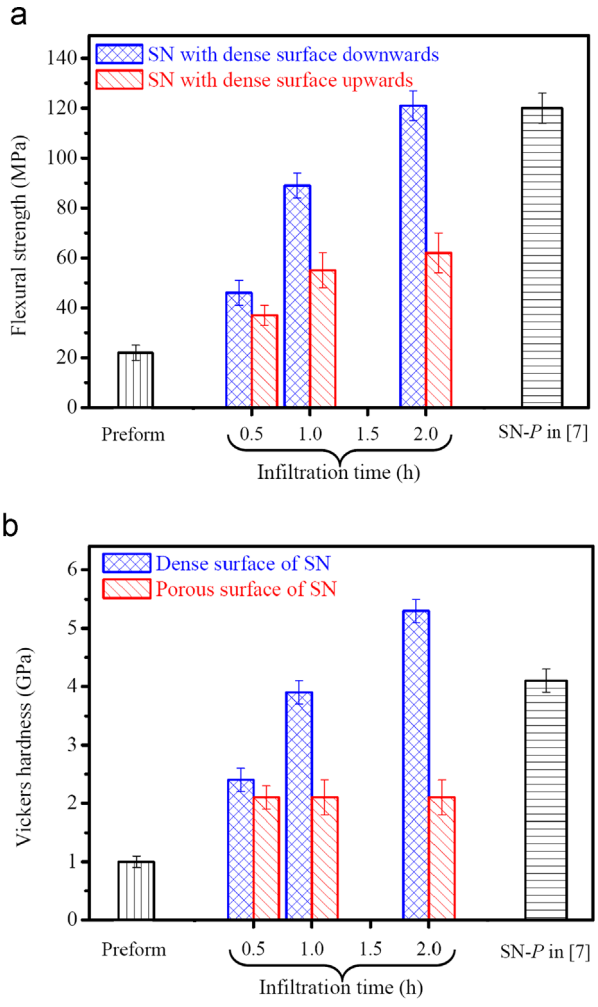

Fig. 6. (a) Flexural strength and (b) Vickers hardness of SN-*n*.

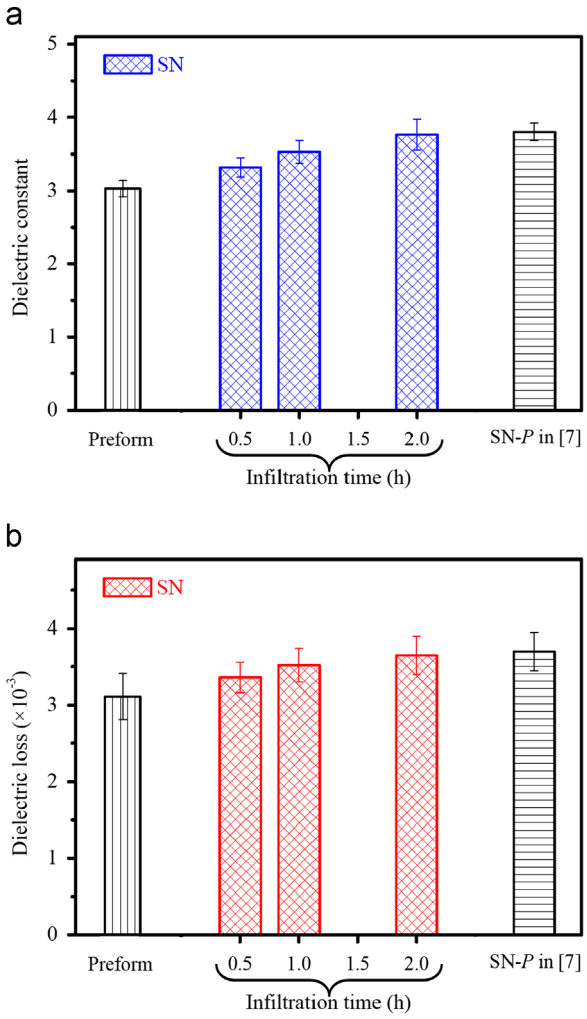

Fig. 7. (a) Dielectric constant and (b) dielectric loss of SN-*n*.

the silica gel will deposit only in the pores at the upside surface of the preforms and there is no more silica gel deposit in the pores at the downside surface of the preforms. As shown in Fig. 6(b), with the increase of infiltration time from 0.5 to 2.0 h, the Vickers hardness of the dense surface of SN-*n* increases obviously from 2.4 to 5.3 GPa, while the Vickers hardness of the porous surface of SN-*n* remains unchanged at 2.1 GPa. Inferred from the above results, the dense surface improves the resistance of SN-2.0 not only to moisture but also to mechanical shock. As shown in Fig. 7, with the increase of infiltration time from 0.5 to 2.0 h, the dielectric constant of SN-*n* increases slightly from 3.32 to 3.76 with the dielectric loss increasing little from 3.36×10^{-3} to 3.65×10^{-3}.

For comparison purpose, the mechanical and dielectric properties of the porous Si_3N_4–SiO_2 ceramic fabricated in our previous work (SN-*P*) [7] are also given in Figs. 6 and 7. As to a porous material, the dielectric properties are much affected by porosity, and the higher porosity leads to lower dielectric constant and loss [13,14]. The total porosity of SN-2.0 is 27.4%, which is higher than that (23.9%) of SN-*P* [7], so SN-2.0 possesses the lower dielectric constant and loss than SN-*P*. However, Due to the well-bonding of Si_3N_4 particles and dense surface, SN-2.0 possesses the higher flexural strength and Vickers hardness than SN-*P*.

4. Conclusions

In this study, porous Si_3N_4–SiO_2 ceramics with dense surface and gradient pore distribution were fabricated by a technique combining oxidation–bonding, sol–gel directional infiltration and sintering. The sol–gel infiltration time has great effect on the mechanical and dielectric properties of porous Si_3N_4–SiO_2 ceramics. With the increase of infiltration time, the porous Si_3N_4–SiO_2 ceramics improve obviously in mechanical properties because of the well-bonding of Si_3N_4 particles, and show low dielectric constant and loss due to their high porosity. With the increase of infiltration time from 0.5 to 2.0 h, the flexural strength increases obviously from 46 to 121 MPa when the dense surface is downward during the test and increases from 37 to 62 MPa when the dense surface is upward during test, the Vickers hardness of the dense surface increases obviously from 2.4 to 5.3 GPa with the Vickers hardness of the porous surface remains unchanged at 2.1 GPa, the dielectric constant increases slightly from 3.32 to 3.76 with

the dielectric loss increasing little from 3.36×10^{-3} to 3.65×10^{-3}.

The porous Si_3N_4–SiO_2 ceramics fabricated in the present work are promising good electromagnetic wave transparent material that can be used as radomes or antenna windows. Importantly, if the radomes and antenna windows are fabricated from the porous Si_3N_4–SiO_2 ceramics with dense surface outwards, the radomes and antenna windows will possess obviously improved resistances to moisture and mechanical shock.

Acknowledgment

The authors gratefully acknowledge the financial support from the National Natural Science Foundation of China (51209177) and the Special Financial Grant from the China Postdoctoral Science Foundation (2013T60891). This work was also supported by the Financial Grant for Science and Technology Young Star from Shaanxi Province (2013KJXX-14), the Basic Research Fund of Northwest A&F University (QN2012024) and the Dr. Scientific Start-up Funds of Northwest A&F University (2011BSJJ083).

References

[1] S.Q. Ding, Y.P. Zeng, D.L. Jiang, Oxidation bonding of porous silicon nitride ceramics with high strength and low dielectric constant, Materials Letters 61 (2007) 2277–2280.

[2] G.W. Wen, G.L. Wu, T.Q. Lei, Z.X. Guo, Co-operative enhancement of fused silica and BN ceramics for high-temperature dielectric applications, Journal of the European Ceramic Society 20 (2000) 1923–1928.

[3] J. Barta, M. Manela, R. Fischer, Si_3N_4 and Si_2N_2O for high performance radomes, Materials Science and Engineering 71 (1985) 265–272.

[4] J.D. Walton, Reaction sintered silicon nitride for high temperature radome applications, American Ceramic Society Bulletin 53 (1974) 255–258.

[5] J.S. Lyons, T.L. Starr, Strength and toughness of slip-cast fused silica composites, Journal of the American Ceramic Society 77 (1994) 1673–1675.

[6] C.M. Xu, S.W. Wang, X.X. Huang, J.K. Guo, Processing and properties of unidirectional SiO_{2f}/SiO_2 composites, Ceramics International 33 (2007) 669–673.

[7] X.M. Li, X.W. Yin, L.T. Zhang, L.F. Cheng, Y.C. Qi, Mechanical and dielectric properties of porous Si_3N_4–SiO_2 composite ceramics, Materials Science and Engineering A 500 (2009) 63–69.

[8] X.M. Li, X.W. Yin, L.T. Zhang, T.H. Pan, Microstructure and properties of porous Si_3N_4 ceramics with a dense surface, International Journal of Applied Ceramic Technology 8 (2011) 627–636.

[9] X.M. Li, L.T. Zhang, X.W. Yin, Effect of chemical vapor deposition of Si_3N_4, BN and B_4C coatings on the mechanical and dielectric properties of porous Si_3N_4 ceramic, Scripta Materialia 66 (2012) 33–36.

[10] X.M. Li, X.W. Yin, L.T. Zhang, S.S. He, The devitrification kinetics of silica powder heat-treated in different conditions, Journal of Non-Crystalline Solids 354 (2008) 3254–3259.

[11] W.T. Sweeney, Cristobalite for dental investment, Journal of the American Dental Association 20 (1933) 108–119.

[12] M.K. Naskar, M. Chatterjee, A. Dey, K. Basu, Effects of processing parameters on the fabrication of near-net-shape fibre reinforced oxide ceramic matrix composites via sol–gel route, Ceramics International 30 (2004) 257–265.

[13] R. Heidinger, S. Nazare, Influence of porosity on the dielectric properties of AlN in the range of 30–40 GHz, Powder Metallurgy International 20 (1988) 30–32.

[14] S.J. Penn, N.M. Alford, A. Templeton, X.R. Wang, M.S. Xu, M. Reece, K. Schrapel, Effect of porosity and grain size on the microwave dielectric properties of sintered alumina, Journal of the American Ceramic Society 80 (1997) 1885–1888.